Journal of Power Sources 195 (2010) 994–1000

Contents lists available at ScienceDirect

Journal of Power Sources

journal homepage: www.elsevier.com/locate/jpowsour

Photon-assisted synthesis of ultra-thin yttria-doped zirconia membranes: Structure, variable temperature conductivity and micro-fuel cell devices

Masaru Tsuchiya, Bo-Kuai Lai, Alex C. Johnson, Shriram Ramanathan*

Harvard School of Engineering and Applied Sciences, Harvard University, Cambridge, MA 02138, USA

ARTICLE INFO

Article history:
Received 5 August 2009
Received in revised form 26 August 2009
Accepted 27 August 2009
Available online 2 September 2009

Keywords:
Yttria-doped zirconia
Ionic conductivity
Micro-solid oxide fuel cells
Photon-assisted processing
Oxide thin films

ABSTRACT

We report on the synthesis and functional properties of nanoscale (~50 nm) dense Y-doped zirconia (YDZ) electrolyte thin films by photon-assisted oxidation of Zr–Y precursor alloy thin films. Crystalline zirconia films with grain size of ~5 nm were successfully grown at room temperature by oxidation under ultra-violet (UV) photon irradiation. Microstructure of the films was characterized by transmission electron microscopy. The electrochemical conductivity of UV grown YDZ electrolytes was investigated over a broad range of temperatures using Pt electrodes as a function of yttria doping concentration. The slightly lower electrical conductivity in UV grown films at intermediate temperature range (400–550 °C) is consistent with previous reports on oxygen defect annihilation under photo-excitation. Micro-fuel cells utilizing such ultra-thin YDZ membranes yielded ~12 mW cm^{-2} power density at 550 °C. The results are of potential relevance in advancing low temperature ultra-thin oxide membrane synthesis for energy applications.

1. Introduction

A thermal photo-excitation during oxidation of precursor alloys is a promising low temperature route for the synthesis of ultra-thin oxides. Particularly, ultra-violet (UV) photon illumination introduces photochemical reactions producing active oxygen species, leading to enhanced oxygen-related kinetics even at room temperature [1,2]. In previous studies, UV-assisted growth has been successfully used to enhance oxidation rate [3–7], oxygen concentration [8,9], crystallinity [10–12], and electrical properties [13–16] of ultra-thin oxide thin films at low temperature. Among various technological applications of nanoscale thin films, micro-solid oxide fuel cells (μSOFC) have been gaining increasing attention in recent years [17–22]. The use of nanoscale electrolytes can result in a decrease of ohmic resistance; thereby possibly an attractive option to lower the SOFC operation temperature down to <600 °C [23]. Presently, various deposition techniques for the synthesis of ultra-thin oxide electrolytes are being explored [24–28], and so far to the best of our knowledge, photon-assisted oxidation of precursor alloys and their conductivity properties has not been reported. UV oxidation is an unique approach since it can enable formation of dense conformal ultra-thin crystalline oxide films with atomically tailored stoichiometry at near room temperatures. Such low temperature synthesis is particularly attractive for μSOFC applications because it introduces minimal effect from unwanted mixing and degradation. Furthermore, low temperature selective enhancement of anion kinetics is an attractive method to investigate the role of oxygen non-stoichiometry in nanometer scale materials where significant differences in structural, electrochemical, and mechanical properties have been observed [29–31]. In this article, we report on the synthesis, structure, and high temperature electrochemical properties of yttria-doped zirconia (YDZ) thin films grown by ultra-violet (UV) oxidation of Zr–Y metal alloys and demonstrate elementary micro-fuel cells using this approach.

2. Experimental

2.1. Film growth

A custom-designed sputtering system fitted with a load-lock chamber capable of *in situ* UV oxidation experiments in controlled oxygen partial pressure and temperature was used in this study [32]. Substrates were cleaned by acetone and ethanol for 5 min each, and then treated with buffered HF (2%) for 2 min followed by de-ionized water cleaning before loading into the chamber. Zr–Y metal alloy films were grown by magnetron co-sputtering on Si (1 0 0) substrates at room temperature in sputtering main chamber. Argon was used as the process gas and the pressure was kept at 5 mTorr during the deposition. The composition ratio of Zr/Y was controlled by changing the gun power (100–150 W for Zr, 5–20 W for Y) during the deposition. Yttria (Y_2O_3) dopant concentration investigated in this study ranged from 0 mol.% to 15 mol.%. After

* Corresponding author.
E-mail address: shriram@seas.harvard.edu (S. Ramanathan).

0378-7753/$ – see front matter © 2009 Elsevier B.V. All rights reserved.
doi:10.1016/j.jpowsour.2009.08.072

~3–4 nm of Zr–Y precursor alloy was grown on the substrates, the samples were transferred to a load-lock chamber and oxidized under UV exposure for 15 min at room temperature in 100% O_2 ambient at ~1 atm. The resultant oxide thickness was ~5 nm, which corresponds to the self-limiting thickness of Zr metal thin films at room temperature grown under UV [33]. A low pressure Hg lamp emitting primarily 254 nm and 185 nm radiation was used as the photon source in this study. After UV oxidation, the load-lock chamber was immediately pumped down to ultra-high vacuum and samples were transferred back into the main chamber for further growth. This process was repeated up to 10 times, followed by post-deposition UV irradiation for 1 h in air. Typical film thickness used in this study was nearly 50 nm.

2.2. Characterization

Film microstructure was characterized by transmission electron microscopy (TEM). Samples were mechanically ground and dimpled down to 10–20 μm, and then thinned to electron transparency by Ar^+ ion beam milling. JEOL 2100 was used in bright field and dark-field imaging as well as selected area diffraction patterns (SAED). Energy dispersive X-ray spectroscopy (EDS) and high-angle annular dark-field imaging (HAADF) were performed in STEM mode using JEOL 2010F.

Electrical measurements were performed by ac impedance spectroscopy using a Solartron electrochemical system (SI 1287 Electrochemical Interface and SI 1206 Impedance Gain-Phase Analyzer) in the frequency range of 1 Hz to 300 kHz. Pt paste was used for high temperature conductivity measurement (700–925 °C), while micro-patterned electrodes were used for low temperature conductivity measurements (<500 °C). Samples for high temperature conductivity measurement were pre-annealed at 885 °C in air for 1 h to stabilize Pt electrodes.

Micro-patterned electrodes were fabricated by dc sputtering of Pt at 250 W in 75 mTorr Ar plasma on photo-lithographically created mask templates. The growth conditions for the Pt electrodes have been described elsewhere [34]. Fuel cell devices were fabricated on silicon wafers using photolithography, etching and thin film deposition. Ten 100 μm × 100 μm active devices were fabricated on 1 cm × 1 cm square Si wafers. Si wafers were coated with low-stress LPCVD silicon nitride on both sides, followed by the deposition of ~50 nm YDZ layers by UV oxidation (described above) and $La_{0.6}Sr_{0.4}Co_{0.8}Fe_{0.2}O_{3-\delta}$ (LSCF) films by rf-sputtering at room temperature. LSCF film deposition was conducted at room temperature for 25 min at a gun power of 60 W in 5 mTorr Ar plasma. We have previously reported on the structure and high temperature conductivity of ultra-thin LSCF cathodes synthesized by this approach [35,36]. Square patterns were created on the backside through a photomask and silicon nitride in etched holes was etched by reactive ion etch (RIE) with O_2 and CF_4. After RIE, the Si wafer was etched in KOH to form pyramidal wells. Front side nitride layer was etched by RIE and a porous Pt anode was sputtered at 250 W for 15 min in 75 mTorr Ar plasma.

3. Results and discussion

3.1. Microstructure

A cross-sectional micrograph taken from as-grown Y-doped zirconia (with 7.5 mol.% Y_2O_3 concentration) is shown in Fig. 1. The film is crystalline with randomly oriented grains of ~5 nm size. The as-deposited grain size was nearly independent of Y doping concentration as seen from a comparison of undoped, 4.6 mol.%, and 7.5 mol.% yttria-doped zirconia thin films shown in Fig. 2 (a), (b), and (c), respectively. Cubic phase was observed even in films with 4.6 mol.% of yttria doping as we have reported earlier [32]. The formation of cubic phase at yttria doping concentration lower than 8–10 mol.% has been observed in nanoscale systems and most likely from its large surface-to-bulk ratio and limited nucleation kinetics in the low temperature synthesized films [37–41].

High-resolution TEM micrograph and corresponding dark-field and electron diffraction patterns of: (a) as-grown $Zr_{0.80}Y_{0.20}$ metal thin films, (b) after room temperature UV oxidation (11.3 mol.% YDZ), and (c) after 900 °C 1 h annealing in air are shown in Fig. 3.

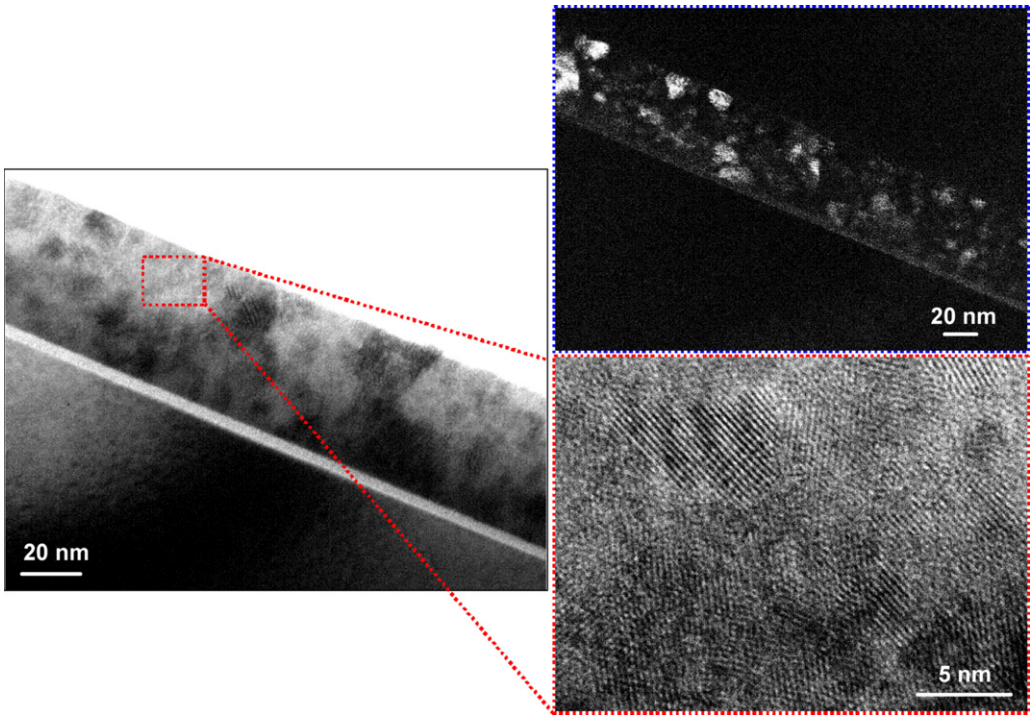

Fig. 1. Cross-sectional TEM micrograph of 7.5 mol.% doped YDZ film as-grown under photo-excitation.

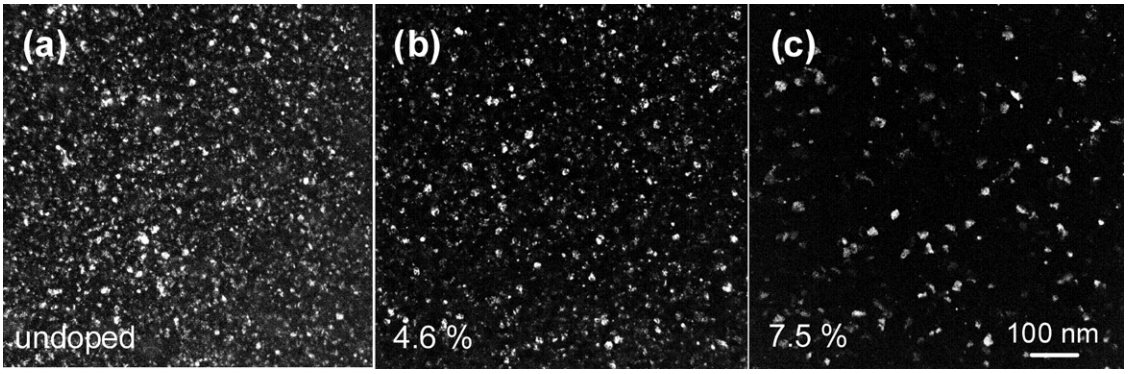

Fig. 2. Plan view dark-field TEM micrograph of UV grown (a) undoped, (b) 4.6 mol.% and (c) 7.5 mol.% yttria-doped zirconia films at room temperature. The scale bar for the three figures are identical.

The as-grown precursor alloy thin films had crystalline grains of ~5 nm embedded in poorly crystalline matrix as shown in Fig. 3(a), which were oxidized into cubic zirconia within 15 min under UV illumination at room temperature (Fig. 3(b)) [32]. The oxidation of Zr–Y alloy is clear from the different diffraction ring radii. After annealing at 900 °C for 1 h, the grains were highly crystalline with sharp boundaries as seen in the high-resolution image in Fig. 3(c). Crystalline structure of YDZ after annealing was likely a mixture of cubic and tetragonal phase, since the tetragonal (1 1 2) peak was also seen in the diffraction pattern along with ring pattern corresponding to the cubic phase. Observation of the tetragonal phase when annealed in oxygen rich ambient is consistent with previous reports on metastable phase stabilization in ultra-thin zirconia films wherein tetragonal phase formation becomes favorable with an increase in oxygen concentration [41–44]. Sharp grain boundaries with no pin holes were seen in the cross-sectional TEM micrograph of the identical film shown in Fig. 4. Energy dispersive X-ray microanalysis (EDS) elemental mapping and annular dark-field image (Z-contrast) of UV grown film obtained by scanning transmission electron microscopy (STEM) are shown in Fig. 5. The distribution of each element is nearly uniform throughout the film. This uniform distribution was confirmed for various yttria doping concentrations. A sample with highest concentration of yttria (14.6 mol.%) is shown in Fig. 5 as a representative case.

3.2. High temperature electrochemical properties (>700 °C)

High temperature electrochemical properties were studied by impedance spectroscopy with porous Pt electrodes. Electrochemical impedance spectra taken from 11.3 mol.% yttria-doped zirconia film measured at 925, 885 and 845 °C are shown in Fig. 6(a). The plots show one semicircular arc with a low frequency feature due to the ion blocking effect of electrode interfaces, similar to measurements on thin film oxides in an in-plane geometry [45–47]. The conductivity of the film was determined from the low frequency intercept of the semicircular arc with the Z' axis (shown as arrows in the figure). The high temperature conductivity of YDZ grown by UV-assist and thermally grown films was comparable

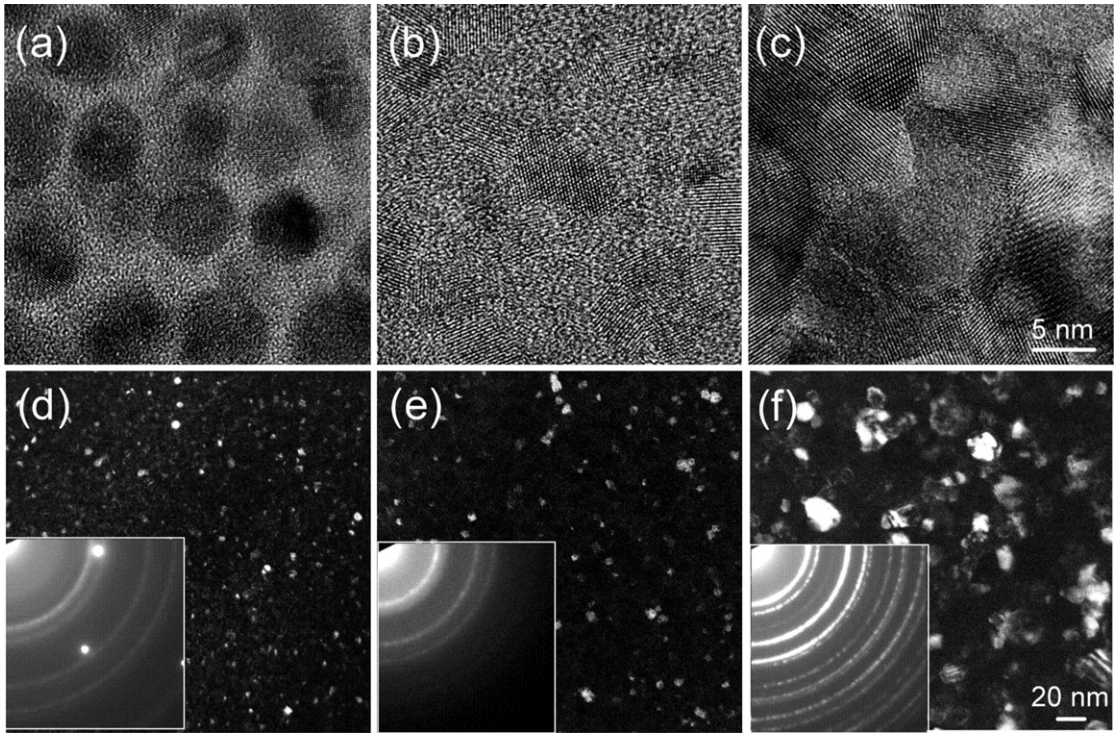

Fig. 3. High-resolution plan view TEM images of: (a) as-grown $Zr_{0.80}Y_{0.20}$ alloy thin films, (b) after room temperature UV irradiation (11.3 mol.% yttria-doped zirconia), and (c) after 900 °C 1 h annealing in 20% O_2 + 80% N_2 ambient. Corresponding dark-field TEM micrographs and selected area diffraction patterns are shown in (d)–(f).

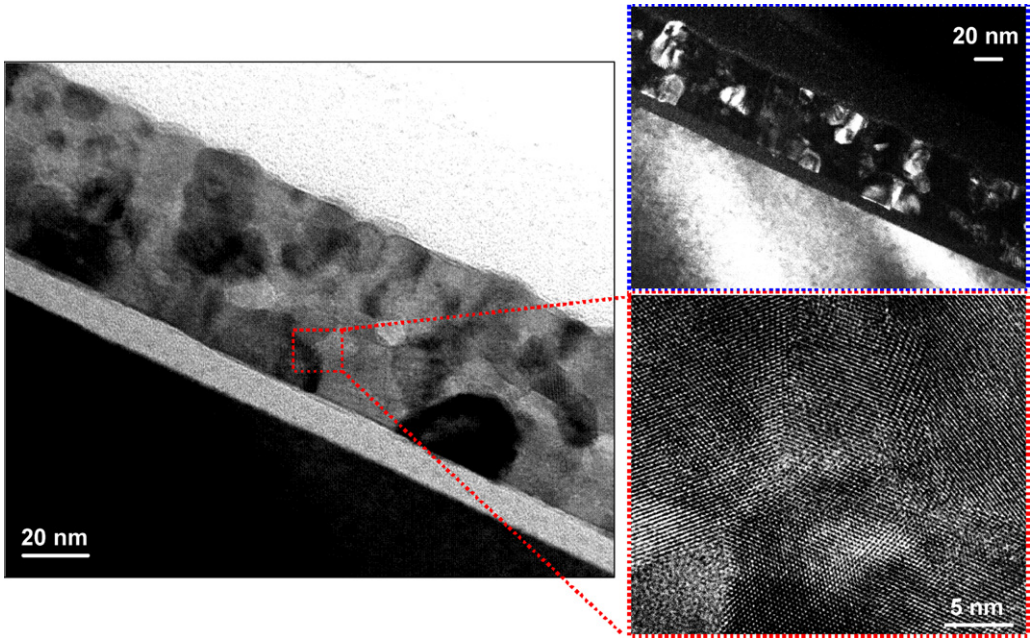

Fig. 4. Cross-sectional TEM micrograph of 11.3 mol.% YDZ after 900 °C 1 h annealing in 20% O_2 + 80% N_2 ambient.

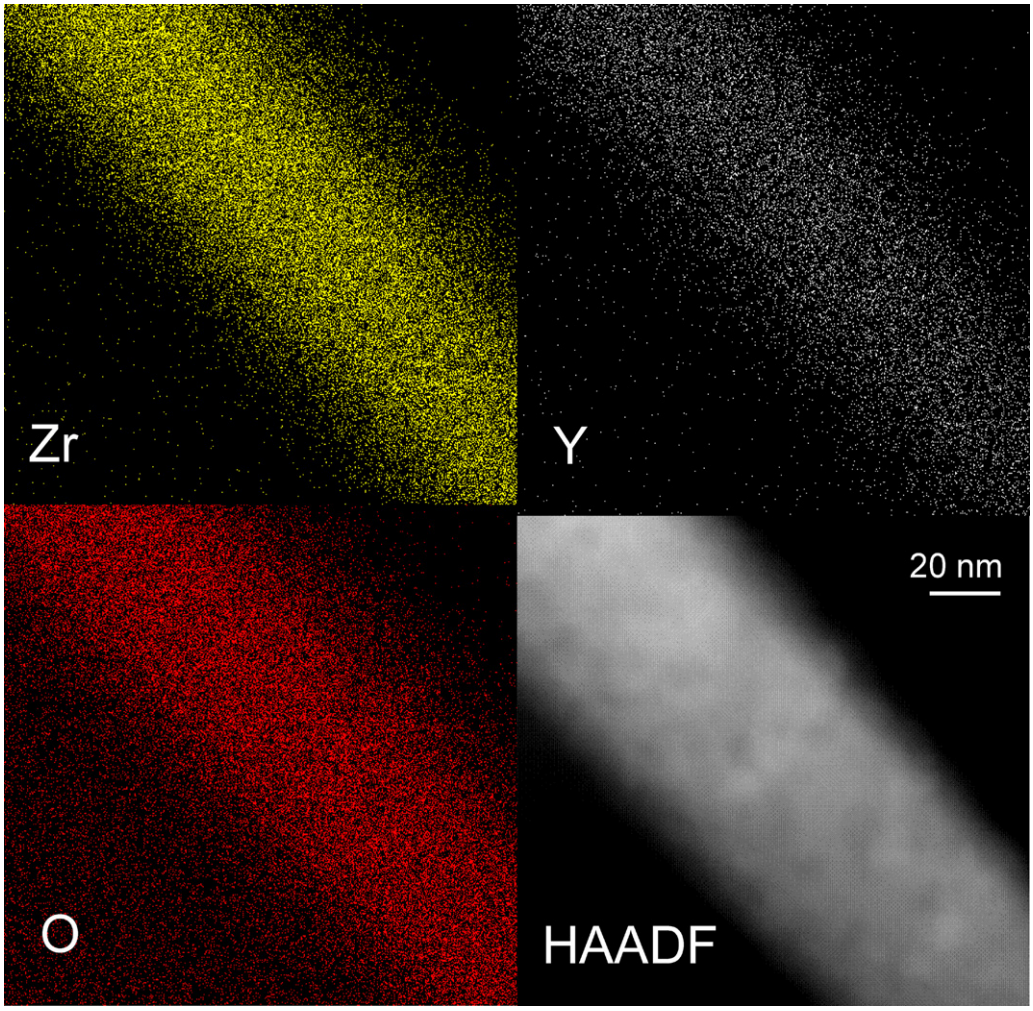

Fig. 5. EDS elemental mapping and Z-contrast image of UV grown 14.6% YDZ film.

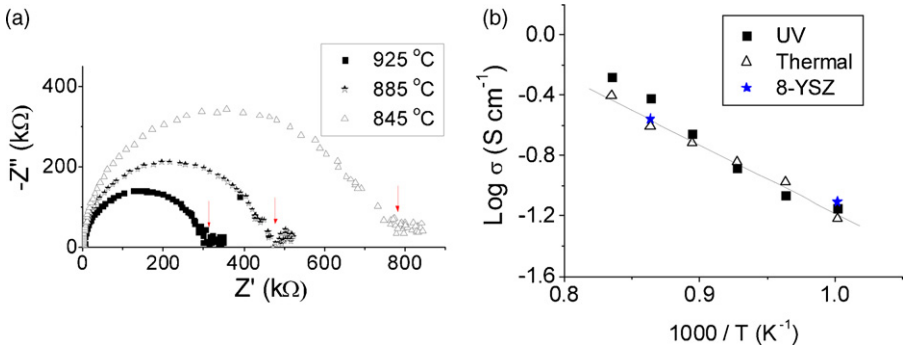

Fig. 6. Nyquist plots measured by electrochemical impedance spectroscopy: (a) UV grown 11.3 mol.% yttria-doped zirconia films measured at 925, 885 and 845 °C and (b) conductivity versus temperature plot of UV and thermally grown YDZ films grown on Al_2O_3 substrate. Conductivity value of ~50 nm thin film YDZ grown by rf-sputtering is plotted as a reference.

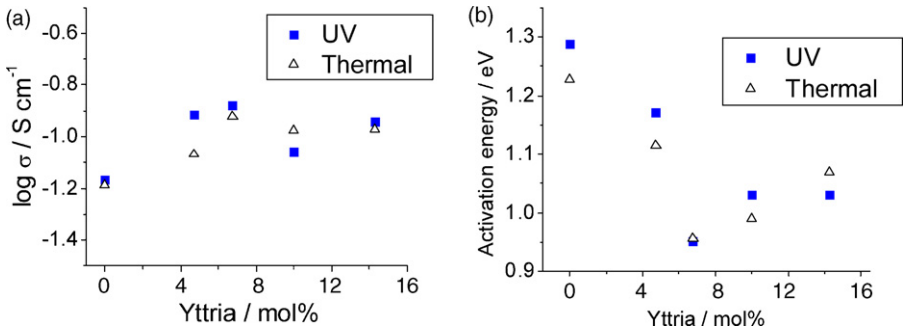

Fig. 7. (a) Activation energy with respect to yttria doping concentration for UV and thermally grown YDZ films, and (b) conductivity versus yttria dopant concentration for UV and thermally grown YDZ films.

as seen in Fig. 6(b). Films synthesized by photon-assisted oxidation have similar activation energy (1.0–1.2 eV) and conductivity values (~0.1 S cm^{-1} at 765 °C) compared to thermally grown and rf-sputter deposited films [43]. These values are also consistent with reported conductivity data for nanoscale thin film YDZ [31,46].

Negligible differences were seen in the activation energy and the absolute conductivity values of the UV and thermally oxidized films at various yttria doping concentration as shown in Fig. 7(a) and (b). Activation energy has a minimum at around 8 mol.% doping and a corresponding conductivity change was also observed. Overall, it is reasonable to conclude that the UV-assisted films have comparable electrochemical properties to conventionally grown films at high temperature (700–900 °C).

3.3. *Intermediate temperature electrochemical properties (<550 °C)*

The conductivity of UV synthesized YDZ at lower temperatures was measured by utilizing micro-patterned electrodes. Porous Pt electrodes were deposited by dc sputtering following photolithography. A detailed account of the electrode fabrication process can be found elsewhere [34]. The conductivity of: (a) 10.0 mol.% and (b) 14.3 mol.% yttria-doped zirconia films grown by UV and thermal oxidation are plotted in Fig. 8. Interestingly, the conductivity of zirconia grown under UV irradiation was found to be slightly lower than that of films grown by conventional oxidation in this temperature range (420–570 °C), while the activation energy in these two cases was nearly identical. This result suggests that the migration mechanism in both cases is similar (i.e., via oxygen vacancies in zirconia [48]), however, the concentration of mobile carriers (i.e., oxygen vacancies) was slightly lower in UV treated films. This is consistent with previous reports on anion defect annihilation under photo-excitation in zirconia thin films [8,32]. The difference in absolute conductivity is much less in 14.3 mol.% YDZ films, likely because of the saturation in effective oxygen vacancy concentration for ionic transport due to dopant association [49]. The effective mobile carrier concentration for ionic transport at 14.3 mol.% yttria doping concentration is expected to be

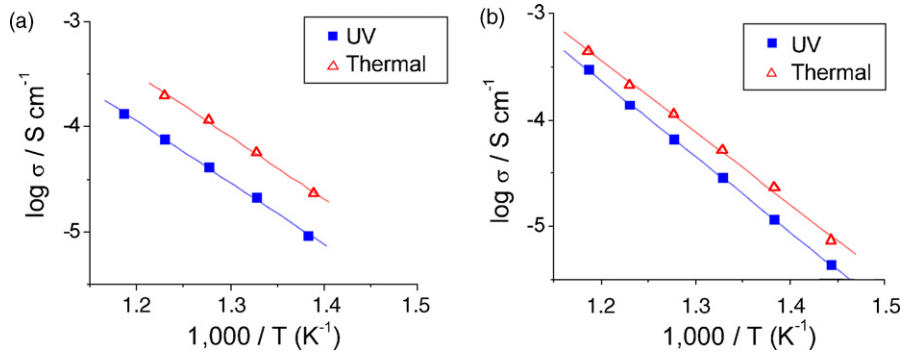

Fig. 8. Low temperature conductivity of YDZ films grown with and without UV irradiation: (a) 10.0 mol.% and (b) 14.3 mol.% yttria doping.

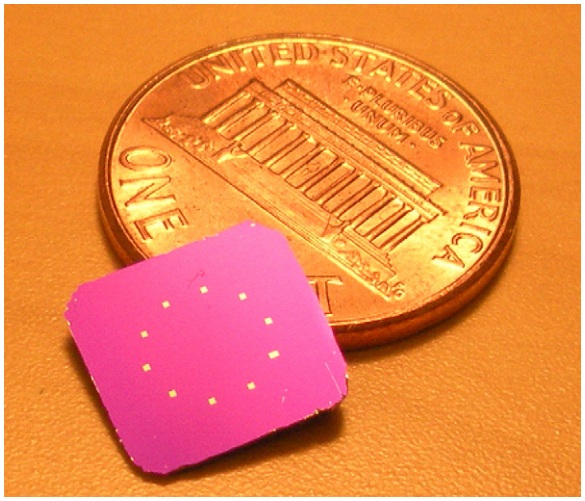

Fig. 9. Optical micrograph of μSOFC test device.

smaller than the value simply expected from the charge neutrality condition $Y_2O_3 = 2Y'_{Zr} + V_o^{\bullet\bullet} + 3O_o^x$, thereby the effect from defect annihilation becomes smaller compared to 10.0 mol.% yttria-doped films.

The results suggest that the UV process is an effective route to tailor oxygen stoichiometry of oxide thin films when the film is oxygen deficient. The difference from UV excitation becomes less significant at higher temperatures and long annealing times, when thermal energy is sufficient to enable kinetic phenomena otherwise uniquely enabled by photo-excitation at lower temperatures. Although the conductivity is slightly lower in UV synthesized films due to defective annihilation, this is perhaps an important result demonstrating the effect of photo-excitation in altering point defect interactions and mobile carrier concentrations in doped-oxides at intermediate temperatures in the range of interest for μSOFC operation. We anticipate this could be of broader relevance towards understanding photon-oxide interactions and athermal approaches to tailor oxygen concentration in nanoscale oxides.

3.4. Micro-solid oxide fuel cells (μSOFC) with UV grown YDZ electrolyte

Thin film solid oxide fuel cells were fabricated utilizing UV grown YDZ electrolytes (containing 10.0 mol.% yttria). The thickness of electrolytes, sandwiched between Pt anode and LSCF cathode, was nearly 50 nm as determined from X-ray reflectivity

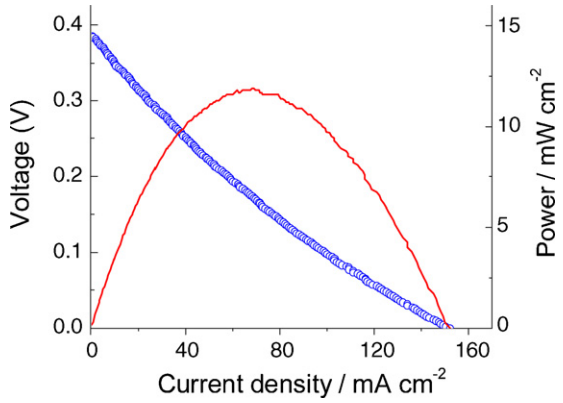

Fig. 11. Current/voltage sweeps from LSCF/YDZ/Pt fuel cells at 550 °C. The electrolyte was a 10.0 mol.% yttria-doped zirconia membrane.

measurements. An optical micrograph of a representative SOFC device is shown in Fig. 9. Ten 100 μm × 100 μm fuel cells with UV-YDZ electrolytes were fabricated as described in Section 2. The optical micrograph of a representative cell before reactive ion etching (RIE) of SiN layer (i.e., YDZ supported on SiN) is shown in Fig. 10(a). This membrane buckled upon the release of SiN supporting layer by RIE (i.e., when the YDZ membrane is free standing) due to the compressive stress introduced during sputter deposition [20] as shown in Fig. 10(b). Functional fuel cells were successfully obtained utilizing UV grown YDZ films as shown in Fig. 11. The open circuit voltage of the cell was ~0.4 V, which is lower than the theoretical value (~1.0 V at 400–600 °C). Current and power density (in cm^{-2}) were calculated based on the assumption that five of 100 μm × 100 μm cells were under operation. The power output was ~12 mW cm^{-2} power density at 550 °C, slightly lower than our previous reported values, due to the low open circuit voltage. The low OCV likely originates from a leak between anode and cathode during measurement. Overall, these initial fuel cell results suggest potential for ultra-thin electrolytes synthesized by photon-assisted oxidation.

4. Conclusions

We have discussed photon-assisted synthesis of ultra-thin YDZ membranes, their conductivity and fuel cell performance. Zr–Y precursor thin films were deposited by co-sputtering, followed by UV-assisted oxidation at room temperature in a custom load-lock chamber. This process was repeated 10 times to grow 50 nm thick YDZ films, since the oxide growth is self-limiting to 5 nm at

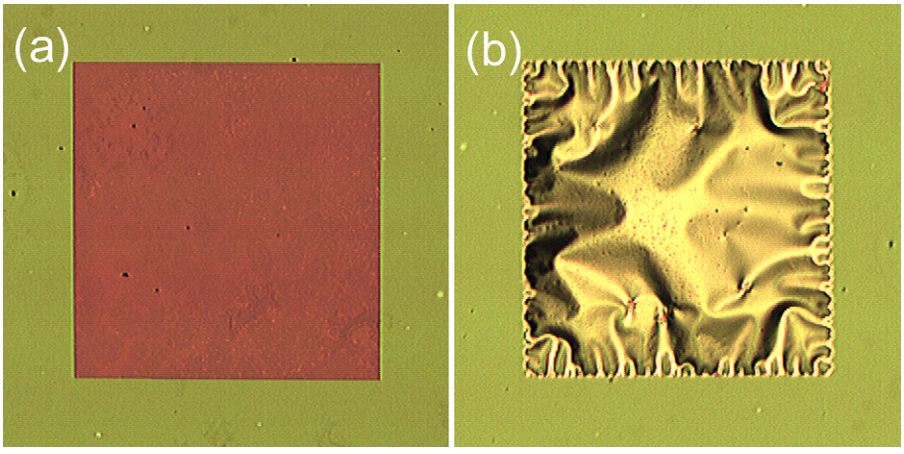

Fig. 10. Optical micrograph of 100 μm × 100 μm square shape cells: (a) before RIE etching and (b) after RIE etching.

room temperature. As-grown Zr–Y alloy films were oxidized into crystalline cubic zirconia with ~5 nm grains under UV illumination in oxygen rich ambient at room temperature. Conductivity studies were performed by ac impedance spectroscopy over the temperature range 400–925 °C. The high temperature conductivity of UV oxides was found to be comparable to the films grown by other vapor deposition methods, while intermediate temperature conductivity was slightly lower. We ascribe this effect to a reduction in mobile carrier concentration under photo-excitation since enhanced oxygen incorporation into the electrolyte membrane likely leads to lesser available oxygen vacancies for carrier transport. Micro-SOFC devices were fabricated using UV-YDZ films and ~12 mW cm^{-2} power density at 550 °C was obtained. We anticipate these results to be of relevance towards advancing photon-assisted synthesis of ultra-thin oxide membranes for energy technologies.

Acknowledgements

The authors acknowledge funding from Global Climate and Energy Project, Si Energy Systems, and Harvard University Center for the Environment that supported this work.

References

[1] H. Okabe, Photochemistry of Small Molecules, Wiley-Interscience Publication, New York, 1978.
[2] M. Tsuchiya, S.K.R.S. Sankaranarayanan, S. Ramanathan, Prog. Mater. Sci. 54 (2009) 981–1057.
[3] A. Kazor, R. Gwilliam, I.W. Boyd, Appl. Phys. Lett. 65 (1994) 412–414.
[4] Y. Ishikawa, T. Shibamoto, T. Uchihara, I. Nakamichi, Jpn. J. Appl. Phys. 30 (1992) L661.
[5] S. Ramanathan, G.D. Wilk, D.A. Muller, C.M. Park, P.C. McIntyre, Appl. Phys. Lett. 79 (2001) 2621–2623.
[6] C.L. Chang, S. Ramanathan, J. Electrochem. Soc. 154 (2007) G160–164.
[7] N. Cabrera, N.F. Mott, Rep. Prog. Phys. 12 (1948) 163–184.
[8] M. Tsuchiya, V. Shutthanandan, M.H. Engelhard, S. Ramanathan, Appl. Phys. Lett. 93 (2008) 263109–263113.
[9] S. Ramanathan, D.A. Muller, G.D. Wilk, C.M. Park, P.C. McIntyre, Appl. Phys. Lett. 79 (2001) 3311–3313.
[10] M. Tsuchiya, S. Ramanathan, Appl. Phys. Lett. 91 (2007) 253104.
[11] V. Craciun, J. Howard, E.S. Lambers, R.K. Singh, D. Craciun, J. Perriere, Appl. Phys. A 69 (1999) S535–538.
[12] H.S. Yang, J. Choi, S.J. Song, R.K. Singh, Electrochem. Solid-State Lett. 7 (2004) C4–6.
[13] C.-L. Chang, S.K.R.S. Sankaranarayanan, M.H. Engelhard, V. Shutthanandan, S. Ramanathan, J. Phys. Chem. C 113 (2009) 3502–3511.
[14] S. Ramanathan, C.M. Park, P.C. McIntyre, J. Appl. Phys. 91 (2002) 4521–4527.
[15] C. Ko, S. Ramanathan, J. Appl. Phys. 103 (2008) 106104.
[16] G.D. Wilk, B. Brar, IEEE Electron Device Lett. 20 (1999) 132–134.
[17] X. Chen, N.J. Wu, L. Smith, A. Ignatiev, Appl. Phys. Lett. 84 (2004) 2700–2702.
[18] J. Fleig, H.L. Tuller, J. Maier, Solid State Ionics 174 (2004) 261–270.
[19] S.J. Litzelman, J.L. Hertz, W. Jung, H.L. Tuller, Fuel Cells 8 (2008) 294–302.
[20] C.D. Baertsch, K.F. Jensen, J.L. Hertz, H.L. Tuller, S.T. Vengallatore, S.M. Spearing, M.A. Schmidt, J. Mater. Res. 19 (2004) 2604–2615.
[21] A. Evans, A. Bieberle-Hütter, J.L.M. Rupp, L.J. Gauckler, J. Power Sources 194 (2009) 119–129.
[22] G.J. LaO, H.J. In, E. Crumlin, G. Barbastathis, Y. Shao-Horn, Int. J. Energy Res. 31 (2007) 548–575.
[23] H. Huang, M. Nakamura, P.C. Su, R. Fasching, Y. Saito, F.B. Prinz, J. Electrochem. Soc. 154 (2007) B20–B24.
[24] G.J. LaO, J. Hertz, H. Tuller, Y. Shao-Horn, J. Electroceram. 13 (2004) 691–695.
[25] Y.I. Park, P.C. Su, S.W. Cha, Y. Saito, F.B. Prinz, J. Electrochem. Soc. 153 (2006) A431–A436.
[26] C.N. Ginestra, R. Sreenivasan, A. Karthikeyan, S. Ramanathan, P.C. McIntyre, Electrochem. Solid-State Lett. 10 (2007) B161–B165.
[27] J.H. Shim, C.C. Chao, H. Huang, F.B. Prinz, Chem. Mater. 19 (2007) 3850–3854.
[28] P.C. Su, C.C. Chao, J.H. Shim, R. Fasching, F.B. Prinz, Nano Lett. 8 (2008) 2289–2292.
[29] J.L.M. Rupp, A. Infortuna, L.J. Gauckler, Acta Mater. 54 (2006) 1721–1730.
[30] T. Suzuki, I. Kosacki, H.U. Anderson, Solid State Ionics 151 (2002) 111–121.
[31] I. Kosacki, C.M. Rouleau, P.F. Becher, J. Bentley, D.H. Lowndes, Solid State Ionics 176 (2005) 1319–1326.
[32] M. Tsuchiya, S. Ramanathan, Appl. Phys. Lett. 92 (2008) 033107.
[33] S. Ramanathan, D. Chi, P.C. McIntyre, C.J. Wetteland, J.R. Tesmer, J. Electrochem. Soc. 150 (2003) F110–115.
[34] A.C. Johnson, B.-K. Lai, H. Xiong, S. Ramanathan, J. Power Sources 186 (2009) 252–260.
[35] B.-K. Lai, A.C. Johnson, H. Xiong, S. Ramanathan, J. Power Sources 186 (2009) 115–122.
[36] B.K. Lai, H. Xiong, M. Tsuchiya, A.C. Johnson, S. Ramanathan, Fuel Cells, in press, doi:10.1002/fuce.200800144.
[37] W. Jung, J.L. Hertz, H.L. Tuller, Acta Mater. 57 (2009) 1399–1404.
[38] M.W. Pitcher, S.V. Ushakov, A. Navrotsky, B.F. Woodfield, G.S. Li, J. Boerio-Goates, B.M. Tissue, J. Am. Ceram. Soc. 88 (2005) 160–167.
[39] R.C. Garvie, J. Phys. Chem. 69 (1965) 1238–1243.
[40] S. Shukla, S. Seal, Int. Mater. Rev. 50 (2005) 45–64.
[41] M. Tsuchiya, A.M. Minor, S. Ramanathan, Phil. Mag. 87 (2007) 5673–5684.
[42] E.G. Rauh, S.P. Garg, J. Am. Ceram. Soc. 63 (1980) 239–240.
[43] M. Tsuchiya, S. Ramanathan, ECS Trans. 13 (2008) 15–22.
[44] M. Tsuchiya, A. Minor, S. Ramanathan, ECS Trans. 11 (2008) 9–16.
[45] S. Kim, J.-W. Son, K.-R. Lee, H. Kim, H.-R. Kim, H.-W. Lee, J.-H. Lee, J. Electroceram, in press, doi:10.1007/s10832-008-9550-y.
[46] A. Karthikeyan, C.L. Chang, S. Ramanathan, Appl. Phys. Lett. 89 (2006) 3.
[47] M. Tsuchiya, A.N. Bojarczuk, S. Ramanathan, Appl. Phys. Lett. 91 (2007) 223101.
[48] A.H. Heuer, L.W. Hobbs, Science and Technology of Zirconia in Advances in Ceramics, vol. 3, American Ceramic Society, Columbus, OH, 1981.
[49] J.W. Fergus, J. Mater. Sci. 38 (2003) 4259–4270.